Oxidation and Stress Corrosion Cracking Initiation of Austenitic Alloys in Supercritical Water

Y. Behnamian[1], Ming.Li[1], J.L. Luo[1], W.X. Chen[1], W. Zheng[2], D.A. Guzonas[3]
[1] Department of Chemical and Materials Engineering, University of Alberta, Alberta, Canada
[2] Materials Technology Laboratory, NRCan, Ottawa, Ontario, Canada
[3] Atomic Energy of Canada Limited, Chalk River Laboratories, Chalk River, Ontario, Canada

Abstract

This study determined the stress corrosion cracking behaviour of austenitic alloys in pure supercritical water. Austenitic stainless steels 310S, 316L, and Inconel 625 were tested as static capsule samples at 500° C for up to 5000 h. After that period, crack initiations were readily observed in all samples, signifying susceptibility to stress corrosion cracking. The microcracks in 316L stainless steel and Inconel 625 were almost intergranular, whereas transgranular microcrack initiation was observed in 310S stainless steel.

1. Introduction

The generation IV, supercritical water (SCW) reactors will be operated at 25 MPa, between 350 °C and 650 °C. While offering promising advantages, the operation in SCW leads to severe material challenges. Components exposed to the SCW are subjected to high stress and heavy oxidation due to the high operating temperature and pressure [1,3], leading to long term degradation phenomena such as creep or stress corrosion cracking (SCC) [1]. Austenitic stainless steels (SS) have high resistance to corrosion in high temperature water, and several researchers have explored oxidation and SCC in austenitic alloys in SCW. Teysseyre et al. [5] studied the susceptibility of austenitic alloys using constant extension rate tensile tests (CERT) in completely deaerated SCW. It was observed that alloy Inconel 625 and 304S SS suffered severe intergranular SCC (IGSCC), both transgranular SCC (TGSCC) and IGSCC were observed in Inconel 690 and 316L SS. Tarnish rupture was reported as a possible mechanism for TGSCC in SCW. Internal oxidation and slip oxidation were proposed to account for general cracking in SCW. Novotny et al. [6] found that the highest temperature for usability of austenitic 316L SS in SCW was 550 °C, and in pure SCW the failure mechanism in the lowest strain rate of 10^{-7} s^{-1} was not IGSCC. Whereas data is still limited regarding the behavior of different metals in SCW. For example, long exposure SCC tests under realistic conditions are necessary to elucidate metal failure mechanisms. In this paper, three different samples of austenitic tubing—310S, 316L, and Inc 625—in capsule form were studied for long time duration and SCC susceptibility of samples in SCW at 500 °C was evaluated by statistical methods.

2. Experimental procedures

310S stainless steel (UNS 31008), 316L stainless steel (UNS 31603), and Inconel 625 (UNSN06625) tubes with an outer diameter of 9.525 mm and a wall thickness of 1.65 mm were purchased from Swagelok. Tubes were manufactured according to the specification defined in ASTM-A-213-09 for stainless steels and ASTM B444 for Inconel 625, and were supplied in solution annealed state. Table 1 shows the chemical composition of alloys in weight percent (wt %).

Table 1

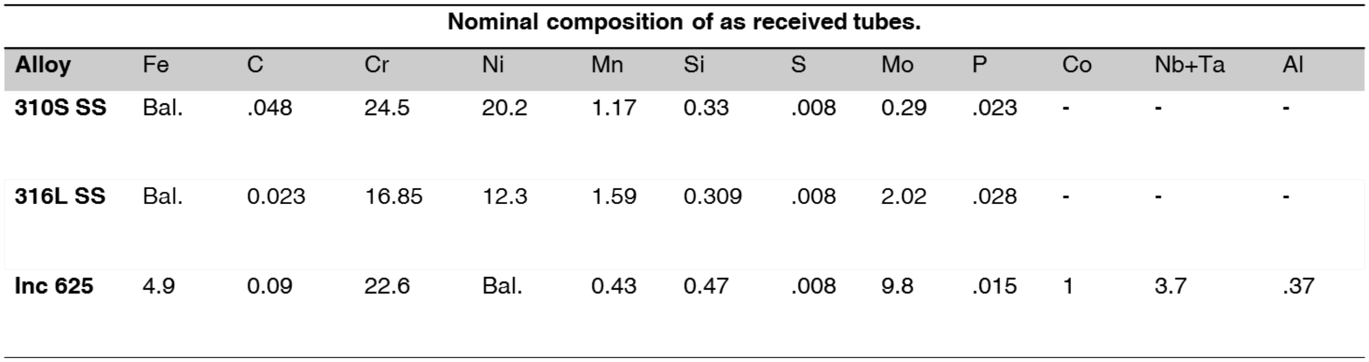

Nominal composition of as received tubes.

Alloy	Fe	C	Cr	Ni	Mn	Si	S	Mo	P	Co	Nb+Ta	Al
310S SS	Bal.	.048	24.5	20.2	1.17	0.33	.008	0.29	.023	-	-	-
316L SS	Bal.	0.023	16.85	12.3	1.59	0.309	.008	2.02	.028	-	-	-
Inc 625	4.9	0.09	22.6	Bal.	0.43	0.47	.008	9.8	.015	1	3.7	.37

Tubes were cut into 10 cm long sections to make capsule samples for SCW exposure. Tube sections were washed in turn with isopropyl alcohol and acetone in an ultrasonic bath before being filled with a specified amount of air-saturated, neutral pH deionised water (DI) containing 8 ppm primary dissolved oxygen (DO). The two ends of each tube were sealed. The sealed tubes were heated at 500 °C up to 5000h. The stress on the tube wall due to this pressure was used to study SCC susceptibility in SCW. Separate capsules were heated to 500 °C for pressure calibration and monitoring. After each test, the water inside the tube was measured. After SCW exposure, tubes were cut into smaller segments. The inner surface of the tubes was plated with a thin layer of Ni to avoid spallation of the oxide film during sample preparation. Samples were mounted with epoxy resin and polished down to 0.5 μm before metallurgical examination. Aqua regia (10 ml) in one third ratios added with 0.05 g ferric chloride was used for etching Inc 625; 100 ml ethanol containing 5% HCl and 0.2 g ferric chloride was used for stainless steel etching. The surface morphologies of the oxide layers on the inner wall of the tubes were examined with a scanning electron microscope (ZEISS EVO-MA15) equipped with an energy dispersive x-ray spectroscope (EDS) in a secondary electron (SE) image mode. Cross-section morphologies were investigated in a backscattered electron (BSE) image mode.

3 Results

3.1 Surface morphology and composition of tube's inner wall oxide layer after SCW exposure.

Fig. 1 shows the inner wall surface morphology of samples after 5000 h exposure. The inner surfaces of tube were covered with crystallite particles; however the density of the crystallite surface was different in each tube. The inner wall surface of sample 310S SS, as shown in Fig. 1a, were covered with fairly large crystallites. In contrast, the crystallites on the inner wall of sample 316L SS shown in Fig. 1b have some unique morphology and seem strongly bonded to the surface. For Inconel 625 (Fig. 1c), the inner surface was featured with some aligned crack-like defects and oxide scales.

X-ray diffraction (XRD) analysis was conducted to identify the surface crystallite components in the tube samples. In samples 310S SS and 316L SS, magnetite was the major component detected, with hematite and chromium oxide present in smaller quantities. The intensity of the magnetite peak suggests that structure covering the tube surface is a coarse, dense crystallite. Based on peak height, the amounts of chromium oxide and hematite detected by XRD on the inner surface of samples 310S SS and 316L SS were not significant. For Inconel 625 (Fig. 1c), the XRD pattern reveals that the major crystallite component in the inner wall is fine nickel oxide.

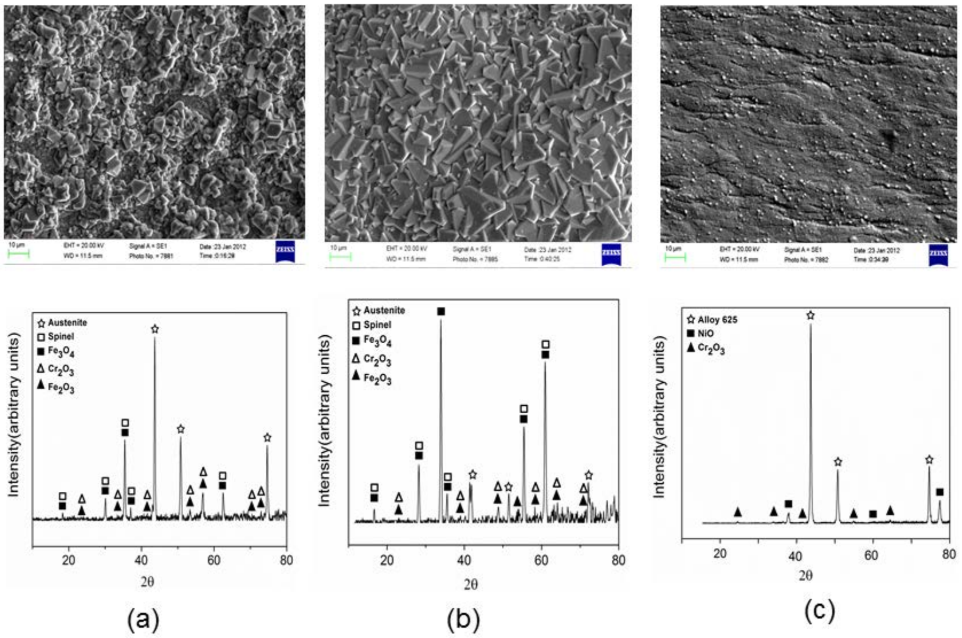

Figure 1 Scanning electron micrographs (SE) and XRD patterns of inner wall oxide layers of 310S SS (a), 316L SS (b), and Inc 625 (c).

3.2 Cross-section micrographs of the oxide layer formed on the inner tube walls after SCW exposure

Fig. 2a and 2b show the results of cross section analysis of 310S SS after exposure to 500 °C for 5000 h. Both the polished and etched images of the same cross-section are comparatively shown. On the polished surface, micro-cracks can be clearly viewed under the oxide scale. On the etched sample, it is further determined that these microcracks were intergranular nature. Similar cross section analysis was also performed on 316L SS. The thickness of the oxide scale on 316L SS was much higher than that on 310S SS. The microcracks were also found on the cross section. These cracks also appeared to be intergranular in nature. Unlike 310SS, the microcracks on 316L SS are generally associated with a thick layer of oxide that was extended to the grain interior. In sample Inc 625 (Fig. 4a and 4b), the microcracks , despite being shallower in compared to 316L SS and 310S SS , show the same trend; nickel depletion and chromium oxidation and enrichment, according to the elemental line scan data.

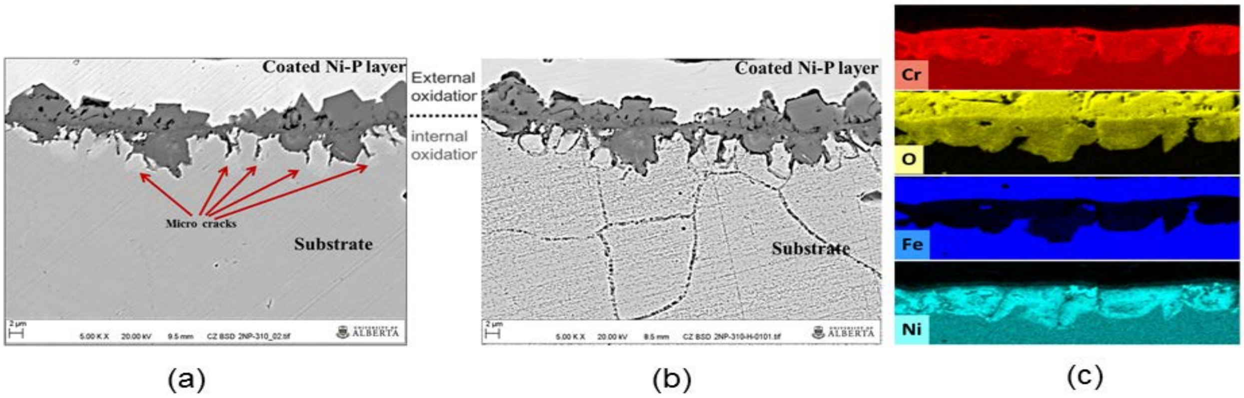

Figure 2 SEM micrographs of tube cross-sections showing oxide layers formed on the inner walls of samples 310S SS, BSE of polished samples (a), BSE of etched samples (b), EDS elemental concentration mapping (c).

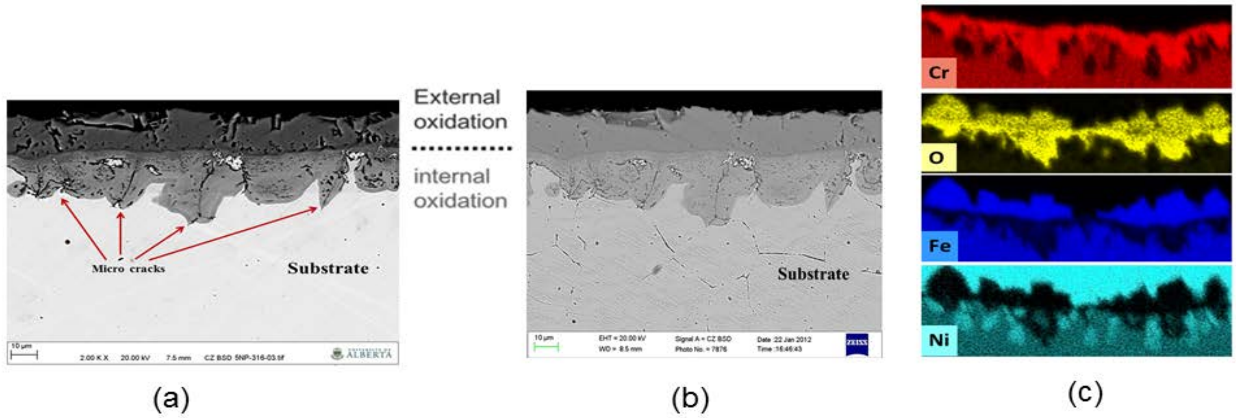

Figure 3 SEM micrographs of tube cross-sections showing oxide layers formed on the inner walls of samples 316L SS, BSE of polished samples (a), BSE of etched samples (b); EDS elemental concentration mapping (c).

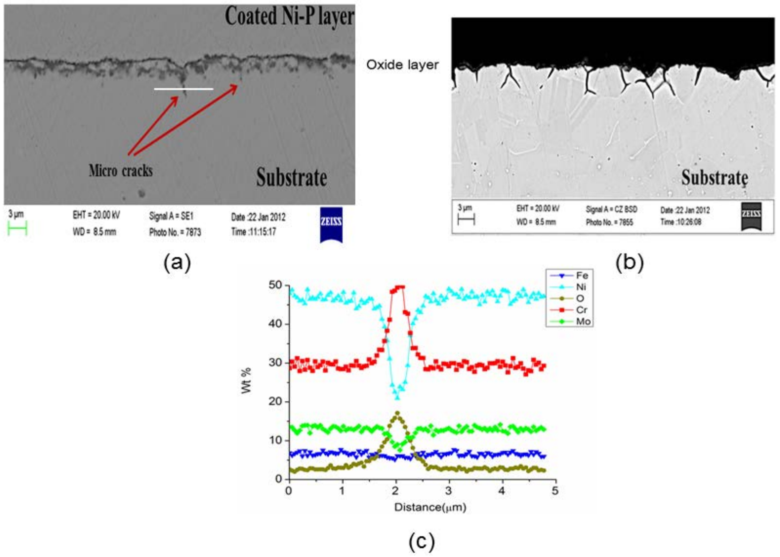

Figure 4 SEM micrographs of tube cross-sections showing oxide layers formed on the inner walls of samples Inconel 625.

4. Discussion

CERT experiments on SSC of metals in supercritical water in accelerated conditions suggested IGSCC might be caused by a dissolution mechanism, an oxidation mechanism, or a combination of these processes [7, 8]. Teysseyre and Was suggested that metal cracking in low density super critical water under conditions such as 25 MPa and 500 °C would take place chemically rather than electrochemically. A thermally activated crack growth rate has also been proposed [5, 9]. Peng et al. reported that constant strain caused the nonstop rupture of an oxide film increasing the crack depth during CERT tests [10]. We tested the SCC of capsule type samples of three different austenitic alloys in supercritical water to further explore the SCC behavior in constant stress.

It has been suggested that the water vapor enhanced corrosion of chromia passivated alloys may occur by several mechanisms. For example, hydrogen increases diffusion of chromium through choromia, forming gaseous iron hydroxide leading to an increase in mass transport and finally the vaporization of chromia in the form of chromium oxide hydroxide (water-vapour-enhanced chromium evaporation) [11]. It has been noted that, in the case of chromium evaporation, the rate of evaporation and the rate of supply is critical to maintain the protective chromia layer [12].

In the present study, the DO concentration of the water in the tubes was 8 ppm before exposure, but oxygen was not supplemented in the tubes during exposure. The oxygen partial pressure was high at the beginning of the exposure but it decreased to a very low level (less than 10 ppb) during exposure. In stainless steel alloys at high oxygen partial pressure, Fe and Cr will oxidize based on their oxygen partial pressures of dissociation [13], but a high oxygen accelerates the water enhanced evaporation of chromia [14]. At this point the fate of the chromia layer depends on whether the supply of chromium is higher or lower than the evaporation rate. Because chromium diffusion was fairly low at 500 °C, and there was a relatively large grain size close to the surface, the supply of chromium would not be expected to last long in the present study, and the oxide would lose part of its protective function [11]. Fe-rich substrate would then be exposed to the SCW directly. Based on the Pourbaix diagram of iron-water in SCW[15], Cook and Olive predicted that if the concentration of Fe is less than 10^{-11} mol/kg, $Fe(OH)_3$ will be stable, and if the concentration of Fe is more than 10^{-6} mol/kg, depending on the oxygen content, Fe_3O_4 or Fe_2O_3 will be stable and an outer Fe-rich oxide layer will form.

After formation of an outer Fe-rich oxide layer, outward diffusion of Fe cations and inward diffusion of oxygen anions would occur[16]. The high affinity of chromium for oxygen facilitated the formation of chromia under the Fe-rich outer oxide layer and grain boundaries (brighter red region of chromium mapping) in samples 310S SS and 316L SS (Fig. 2c, 3c). The lower affinity for oxygen and a slower diffusion rate compared to iron caused nickel to be trapped under the outer part of the oxide (brighter region of nickel mapping) in samples 310S SS and 316L SS (Fig. 2c, 3c).

A comparison of SEM micrographs of tube cross-sections (Fig. 2a,3a) and EDS elemental mapping (Fig. 2c,3c) of 310S SS and 316L SS reveals fairly dense microcracks in 310S SS compared to 316L SS, despite the higher chromium content of 310S SS (Table 1). Asteman et al., studying the stability of chromium protective layers on 310S SS and 304S SS at 600 °C in a H_2O/O_2 mixture, suggested that transition of protective to non-protective behavior of 310S SS in more sudden than 304L SS. Subjected to more sudden nonprotective behavior causes sudden exposure of 310S SS Fe-rich ,Cr-depleted substrate to pure SCW [8] and formation of oxidation pits.

In the case of Inc 625, Ren [17] reported that on the thin oxide surface (less than 1µm) after SCW exposure at 600 °C for 1026 h, grain boundaries were depleted of nickel and enriched in oxygen and chromium. For Inc625 Fig. 4a the micro cracks, initiating from the oxidized surface, analyzed by EDS line scan through the length of white line. The profile of elemental concentration are compatible by Ren's depth profile of ion milled EDS mapping which is suggesting intergranular corrosion and oxidation.

5. Conclusion

Susceptibility to stress corrosion cracking in pure supercritical water at 500 °C of three austenitic alloys was investigated in this study. The alloy most susceptible to microcracks was 316L SS and the least susceptible alloy was Inc 625. The 316L stainless steel and Inconel 625 samples were susceptible to an intergranular type of microcracks. The 310S SS sample was susceptible to transgranular and intergranular microcracks initiation.

6. References

[1] S. Baindur, Materials challenges for the Supercritical Water-Cooled Reactor (SCWR), (2007) 938-949.

[2] T. Abram, S. Ion, Generation-IV nuclear power: A review of the state of the science, Energy Policy, 36 (2008) 4323-4330.

[3] P. Kritzer, Corrosion in high-temperature and supercritical water and aqueous solutions: a review, The Journal of Supercritical Fluids, 29 (2004) 1-29.

[4] H. Ohtaki, T. Radnai, T. Yamaguchi, Structure of water under subcritical and supercritical conditions studied by solution X-ray diffraction, Chemical Society Reviews, 26 (1997) 41-51.

[5] S. Teysseyre, G.S. Was, Stress corrosion cracking of austenitic alloys in supercritical water, Corrosion, 62 (2006) 1100-1116.

[6] R. Novotny, P. Hähner, J. Siegl, P. Haušild, S. Ripplinger, S. Penttilä, A. Toivonen, Stress corrosion cracking susceptibility of austenitic stainless steels in supercritical water conditions, Journal of Nuclear Materials, 409 (2011) 117-123.

[7] K.N. Ryutaro Fujisawa, M.S. Takashi Nishida, Y. Kurata, Y. Watanabe, Cracking susbeptibility of Ni base alloys and 316 stainless steel, NACE, 2005.

[8] E.A. West, M. University of, Influence of local stress and strain on intergranular cracking of 316L stainless steel in supercritical water, 2010.

[9] S. Teysseyre, G.S. Was, Stress corrosion cracking of neutron-irradiated stainless steel in supercritical water, in, 2007, pp. 540-552.

[10] Q.J. Peng, S. Teysseyre, P.L. Andresen, G.S. Was, Stress Corrosion Crack Growth in Type 316 Stainless Steel in Supercritical Water, Corrosion, 63 (2007) 1033-1041.

[11] H. Asteman, J.E. Svensson, L.G. Johansson, Oxidation of 310 steel in H2O/O2 mixtures at 600 °C: the effect of water-vapour-enhanced chromium evaporation, Corrosion Science, 44 (2002) 2635-2649.

[12] H. Asteman, J.E. Svensson, M. Norell, L.G. Johansson, Influence of Water Vapor and Flow Rate on the High-Temperature Oxidation of 304L; Effect of Chromium Oxide Hydroxide Evaporation, Oxidation of Metals, 54 (2000) 11-26.

[13] I.G. Wright, B.A. Pint, An assessment of the high-temperature oxidation behavior of Fe-Cr steel in water vapor and steam, NACE, 2002.

[14] S.N.V.K. Aki, Z.-Y. Ding, M.A. Abraham, Catalytic supercritical water oxidation: Stability of Cr2O3 catalyst, AIChE Journal, 42 (1996) 1995-2004.

[15] W.G. Cook, R.P. Olive, Pourbaix diagrams for the iron–water system extended to high-subcritical and low-supercritical conditions, Corrosion Science, 55 (2012) 326-331.

[16] G.S. Was, S. Teysseyre, Z. Jiao, Corrosion of Austenitic Alloys in Supercritical Water, Corrosion, 62 (2006) 989-1005.

[17] X. Ren, K. Sridharan, T.R. Allen, Corrosion Behavior of Alloys 625 and 718 in Supercritical Water, Corrosion, 63 (2007) 603-612.